2,15-Dibutoxy-6,11-dicyano[6]Helicene: Synthesis, electrochemical, photophysical properties and computational studies

Sondes Raouafi,[a] Mourad Chmeck,[a] Francesca Fontana,[b] Kamel Alimi,[a] Faouzi Aloui[a,*]

[a] *Faculty of Sciences, laboratory of asymmetric synthesis and molecular engineering of organic materials for electronic organics (LR18ES19), University of Monastir, 5019 Monastir-Tunisia.*

[b] .....

* Corresponding author: e-mail address: alouifaouzi0@gmail.com

Abstract. 2,15-Dibutoxy-6,11-dicyano[6]Helicene (**CN-HEL**) has been prepared through a two-step sequence under mild conditions, in an overall 78% yield, starting from 2,7-bis(cyanomethyl)naphthalene as a suitable material. The Helicene has been experimentally characterized and its absorption and photoluminescence (PL) properties have been evaluated showing a strong emission in the blue region of the visible spectrum. A strong absorption is entirely in the UV region (λ_{max} = 290 nm), yet fluorescence occurs at 400 nm. This equates to a Stokes shift of 1.17 eV (9482 cm^{-1}) which is among the large Stokes shifts reported for small molecules making them promising candidates for optoelectronic applications. Furthermore, the ^{1}H NMR, FT-IR, UV-vis and PL spectra were computed by means of the very efficient time-dependent density functional theory (TD-DFT) approach. The computed spectra with two recommended density functionals (PBEPBE and cam/B3LYP) and extended basis sets compare very well with the corresponding experimental data. HOMO and LUMO energy levels were also investigated experimentally, showing an electrochemical band gap of 2.54 eV. Results obtained throughout this work are of great importance and prove the relevance of the target Helicene to be used in a wide range of both existing and new applications such as fluorescence probes and molecular sensors.

Keywords: Helicenes, Photooxidation, Energy levels, Photophysical properties, Quantum chemical calculations.

1. Introduction

Since the discovery of Helicenes by Newmann [1], the area has become an important topic for researchers due to their interesting electronic and photophysical properties which drove them into different fields. The aromaticity and the chirality of Helicenes represent one of the most fascinating topics in science. In order to predict new ideal materials for optoelectronics, understanding of the structure-property relationship of that material is important. In recent

years, plenty of research is focused on structural modification of Helicenes to get high-performance devices and, gratifyingly, significant progress has been made in this regard, which encourages many researchers to widen the exploitation of Helicene-based systems.

Helicenes represent one of the better studied polycyclic aromatic hydrocarbons (PAHs) that have received substantial consideration because of their twisted shape which results from the repulsive steric overlap of the terminal aromatic nuclei. These compounds with their unique π-electron system and their distinctive characteristics include semi-conductivity, photoconductivity, configurational stability and optical absorption in the visible region, led to unprecedented properties and potential applications in chiral discotic liquid crystalline materials [2,3], building blocks for helical conjugated polymers and sensors [4,6] and more fascinatingly as catalysts in asymmetric synthesis [7,8], and recently, as blue emitters in OLEDs and various other optical applications [9-12].

Representative examples of dicyanohelicenes (Fig. 1) like 3,12-dimethoxy-5,6,9,10-tetrahydro-7,8-dicyano[5]Helicene (**DTDH**) [13] and 3,12-dimethoxy-7,8-dicyano[5]Helicene (**DDH**) [14] displayed bright electroluminescence and were found suitable to be used as emissive materials for organic light emitting diodes (OLEDs). Recently, 7,12-dicyano-3,16-dimethoxy[7]Helicene (**1**) has been synthesized and showed a large fluorescence emission rate as well as CPL brightness that indicated a possible potential application as a chiral emitter [15]. Nowadays, the search for efficient blue emitters for OLED devices is an ongoing area of research and other examples of blue-emitting Helicene-containing systems exist [16,17].

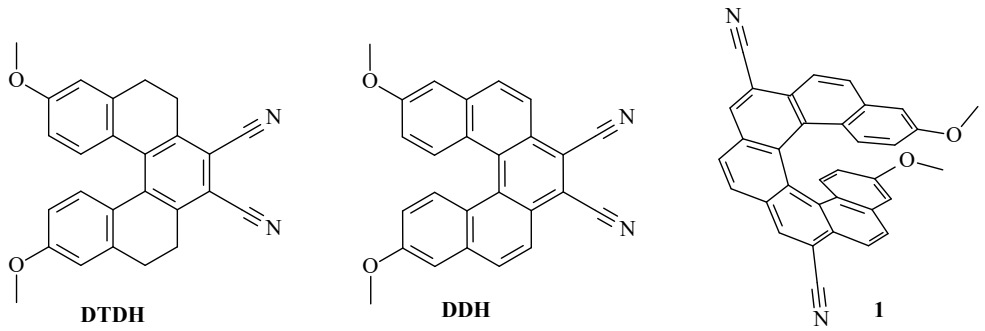

Fig. 1. Representative examples of dicyanoHelicenes as emitters.

Our final goal in the present work is to design and develop a nitrile grafted [6]Helicene derivative which may present interesting optoelectronic properties for a possible application in optoelectronic devices. Herein, the strategy we adopted resides in employing of *Push-Pull* molecule design, which consists of a conjugate *π*-electron system, symmetrically substituted by electron-donor units and electron-acceptor units. In this light, a D-π–A luminophore namely 2,15-butoxy-6,11-dicyano[6]Helicene (**CN-HEL**), bearing two butoxy and two cyano

groups as electron donors and acceptors, was synthesized in a good yield through a short and simple photochemical pathway. The butoxy groups have been appended to improve, among other things, the solubility of the target Helicene in common organic solvents. The redox behavior of **CN-HEL** was investigated by cyclic voltammetry and the optical properties were examined by using UV-vis and photoluminescence spectroscopies.

2. Results and discussion

The synthetic route leading to the target [6]Helicene **CN-HEL** is depicted in Scheme 1. First, we resorted to Knoevenagel reaction conditions, so as to couple the 2,7-bis(cyanomethyl)naphthalene (**2**) to 4-butoxybenzaldehyde in the presence of sodium methoxide in anhydrous methanol which gave the corresponding *α*,*β*-unsaturated nitrile **3** in 93%. **2** has been prepared according to previous procedures [18,19]. Second, we subjected compound **3** to oxidative photocyclization reaction in a dilute solution. The irradiation was performed using 500 W Hg-vapor lamp, on a 150 mg scale par run in 1L of toluene, in the presence of stoichiometric amount of iodine as the oxidizing agent and excess of propylene oxide as hydrogen iodide scavenger. After 9 hours, the desired Helicene (**CN-HEL**) was obtained in 85% yield and an overall 78% yield. No photodimer has been identified nor isolated during this step.

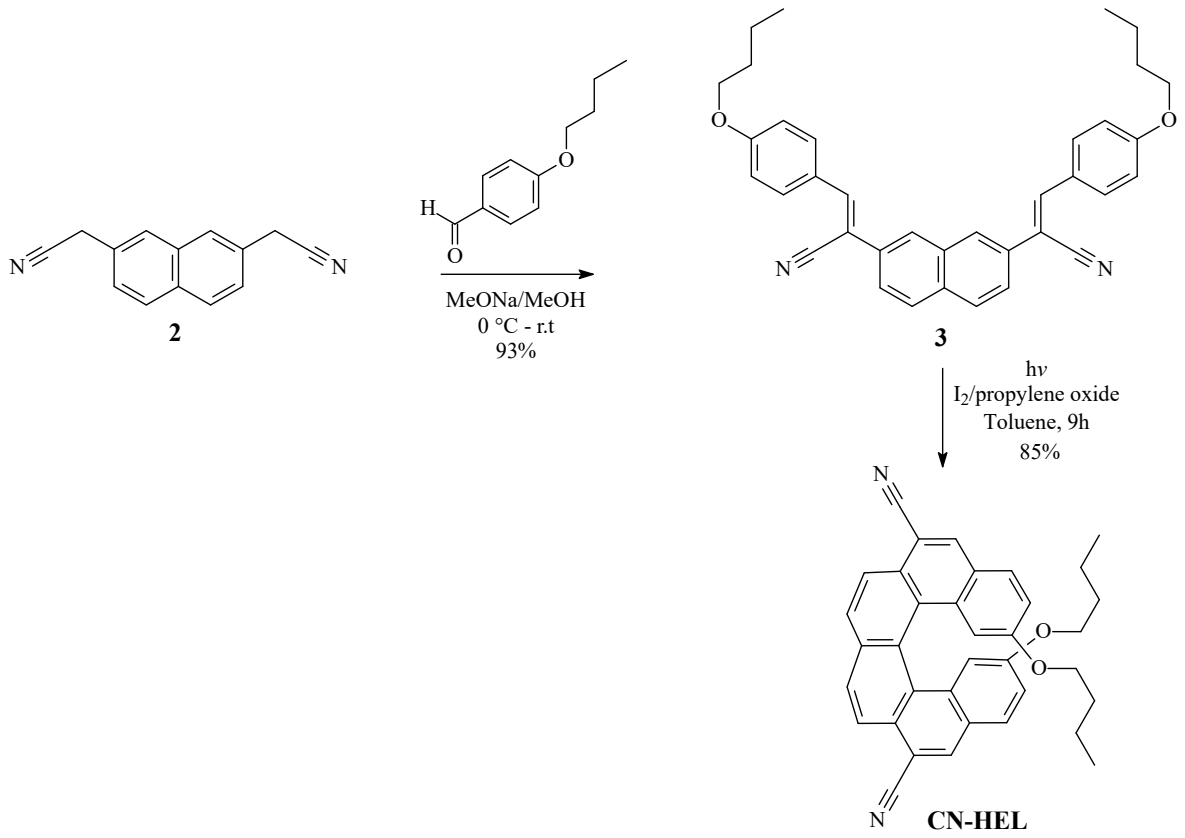

Scheme 1. Synthetic pathway leading to 2,15-dibutoxy-6,11-dicyano[6]Helicene (**CN-HEL**).

The ^{1}H NMR spectrum (Fig. 2) of **CN-HEL** shows a triplet at δ = 0.87 ppm for the two methyl groups and four successive multiplets have also been observed in the range of δ = 0.92−3.17 ppm which are attributable to the methylene groups of the butoxy chains. A set of characteristic singlet at δ = 6.91 ppm was assigned to protons $H_{1/16}$ and a double of doublets at δ = 7.00 ppm (J_1 = 2.4 Hz, J_2 = 8.8 Hz) for $H_{3/14}$, a deshielded singlet at δ = 8.36 ppm for $H_{5/12}$ under the effect of the electron withdrawing cyano groups and a doublet at δ = 8.47 ppm (J = 8.4 Hz) assigned to protons $H_{7/10}$. The deshielding of the doublet may be due to the magnetic anisotropy effects.

The chemical shifts were also calculated using density functional theory (DFT/ PBEPBE (6-31++g(d,p)) with a continuum solvent model for $CDCl_3$, and comparison with experimentally measured chemical shifts are shown in Table 1. For this compound all calculations are in relatively good agreement compared to experimental data and the signals for protons $H_{1/16}$, $H_{3/14}$, $H_{5/12}$ and $H_{7/10}$ are in a good accordance with theoretical signals $H_{52/67}$, $H_{51/66}$, $H_{53/68}$ and $H_{55/69}$.

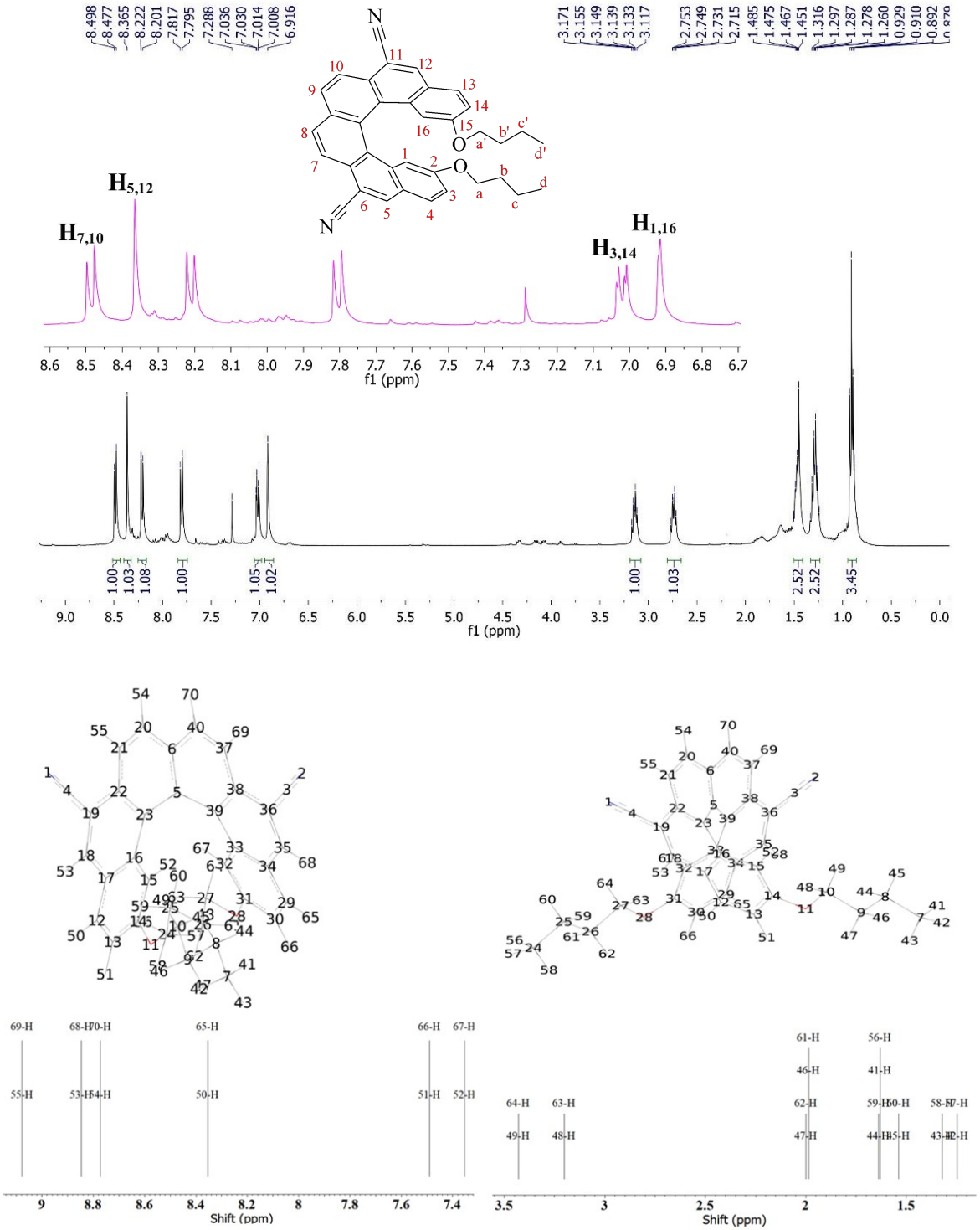

Fig. 2. Experimental (**top**) ^{1}H NMR spectrum ($CDCl_3$, 400 MHz, 298 K) of 2,15-dibutoxy-6,11-dicyano[6]Helicene (**CN-HEL**). (**Bottom**) TD-DFT (PBEPBE/6-31++g(d,p) with a continuum solvent model for $CDCl_3$) calculated data.

Table 1

Selected characteristic experimental and calculated ^{1}H NMR data (δ in ppm) for **CN-HEL**.

Protons	Experimental δ (ppm)	Calculated δ (ppm)
$H_{1/16}$	7.65	7.35
$H_{3/14}$	7.52	7.49
$H_{5/12}$	8.47	8.85
$H_{7/10}$	8.52	9.08

In order to identify the functional group of **CN-HEL,** the obtained material was characterized then by FT-IR spectroscopy in the range 500-3500 cm^{-1}. Else, the theoretical IR spectrum of the optimized chemical structure was calculated with DFT/PBEPBE/6-31++g(d,p) level of theory using dichloromethane as a continuum solvent model. The theoretical spectrum was adjusted with the scale factor 0.988 and presented with an experimental one in Fig. 3. The theoretical infrared spectrum is in good agreement with the experimental data (see Table 2), which indicates a good efficiency of the DFT method at the PBEPBE/6-31++g(d,p) level of theory. Using Gaussview software, the collected functional groups were easily identified. Indeed, for the high-frequency region, C-H stretching vibrations of polyaromatic compounds were observed at 3000-3100 cm^{-1} [20]. Experimentally, the corresponding bands of the title compound are observed in the expected region as 2960 cm^{-1}. Theoretical value computed at 3032 cm^{-1}. The intense IR band observed at 2218 cm^{-1} is assigned to the C≡N stretching vibration, which is presented in the DFT calculated FT-IR spectrum by an intense band vibration located at 2228 cm^{-1}.

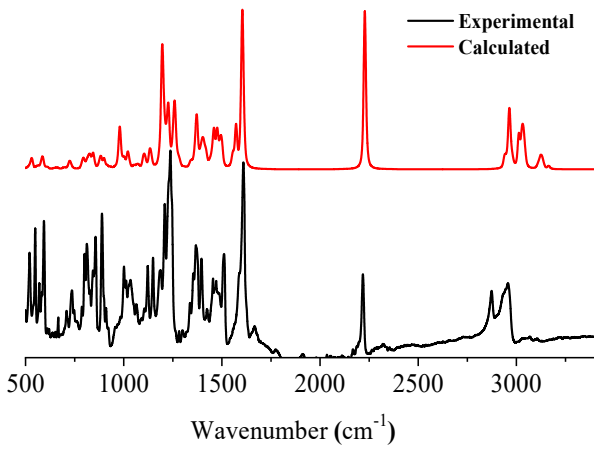

Fig. 3. Experimental and simulated (DFT/PBEPBE/6-31++g(d,p) with a continuum solvent model for CH_2Cl_2) FT-IR spectra of **CN-HEL**.

Table 2

Calculated and experimental vibration frequencies (cm^{-1}) of **CN-HEL**. Frequencies are calculated using DFT/PBEPBE/6-31++g(d,p) with a continuum solvent model for CH_2Cl_2.

Experimental frequency (cm^{-1})	I	Calculated frequency (cm^{-1}) DFT/PBEPBE/6-31++g(d,p)	I	Assignments [20]
517	m	435	w	C-H deformation
711	w	724	w	C-H deformation
797	m	792	w	Phenyl ring vibration
996	m	978	m	C-O stretching
1032	m	1018	w	Aromatic C-H out of plane
1118	m	1100	w	C-H deformation
1186	m	1196	s	C-C deformation
1213	s	1231	m	Aromatic C-H in plane
1240	s	1263	m	Aromatic C-H in plane
1335	w	1344	w	Aromatic C-H in plane
1267	m	1371	m	C-C stretch
1398	m	1403	m	Phenyl ring vibration
1453	m	1457		C-H deformation
1471	m	1475	m	C-C stretch deformation
1489	m	1498	m	C-H deformation
1511	s	1570	m	Phenyl ring vibration
1607	s	1607	s	Phenyl ring vibration
1669	w	1663		Phenyl ring vibration
1730	w	1730		C-H deformation
2218	m	2228	vs	C≡N deformation
2870	m	2962	m	C-H deformation

The UV-vis absorption spectrum of compound **CN-HEL** was recorded in chloroform (C = 1.5 x 10^{-5} mol.L^{-1}), at room temperature, and selected data are summarized in Fig. 4 and Table 3. The experimental spectrum shows the presence of two absorption bands: the first below 400 nm which may be due to π-π* and n-π* transitions of the conjugated aromatic moieties, while the second is in the range 400-450 nm corresponding to intramolecular charge transfer (ICT) between the donor and the acceptor units. Their low intensity is mainly due to the luck of a strong push-pull system and the distorted structure, which hinders the charge flow. The maximum intensity of the ICT band is observed at 426 nm with a moderate molar extinction coefficient of about 1.33 x 10^{-7} L.mol^{-1}.cm^{-1}, while the onset of absorption (λ_{onset}) occurs at 441 nm resulting in an optical band gap energy ($E_{g\text{-}op}$) of 2.81 eV obtained by applying the following formula:

$$E_{g\text{-}op} = hc/\lambda_{onset}$$

$$E_{g\text{-}op}\ (eV) = 1240/\lambda_{onset}$$

Where h represents the Planck constant (6.62607004 x 10^{-34} m^2.kg.s^{-1}), c is the celerity of light (3 x 10^8 m.s^{-1}), and λ_{onset} is the onset wavelength.

To further reveal the effect of different electron donors/acceptors on the photophysical properties and to assign the electron transitions, we calculated UV-vis spectrum of the studied

compound **CN-HEL** by employing time-dependent density functional theory (TD-DFT/cam/B3LYP/6-31++g(d,p)) with a continuum solvent model for $CHCl_3$, which has become a widely used tool to investigate the electronic transition properties [21-23]. The experimental UV-vis absorption spectrum was also reproduced to reliably assign electron transitions. The high energy region displays a transition around 363 nm (using TD-DFT/cam/B3LYP/6-31++g(d,p)) and 372 nm using TD-DFT/PBEPBE-6-31++g(d,p), resulting from HOMO-1 to LUMO and HOMO to LUMO+1 transitions with an oscillator strength of 0.0001 and agrees with the experimentally recorded absorption band (365 nm). This absorption band is even weak ($f < 0.01$) and hardly detectable from the UV-vis spectrum. In addition to this weak $S_0 \rightarrow S_1$ transition, the calculated UV-vis spectrum shows a moderate absorption band at 345 nm resulting from $S_0 \rightarrow S_2$ transition with oscillator strength of 0.078 which is governed by the contribution from HOMO to LUMO (56%). Experimental results show that the maximum wavelength (290 nm) is shifted by 5 to 15 nm with respect to the calculated ones, 285 nm using TD-DFT/PBEPBE/6-31++g(d,p) and 275 nm (using TD-DFT/cam/B3LYP/6-31++g(d,p)).

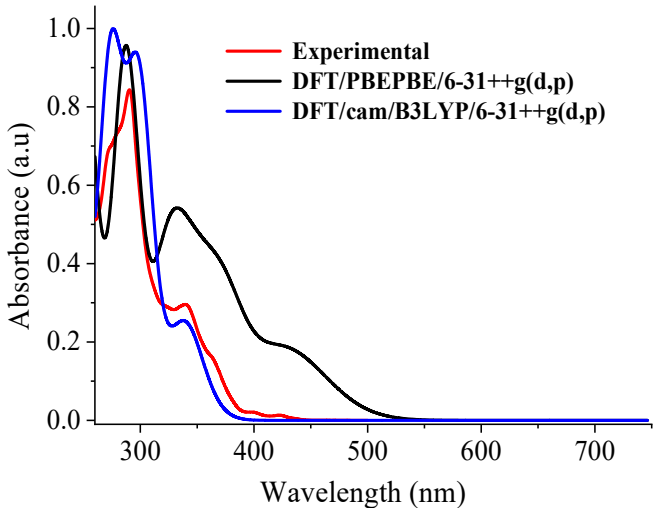

Fig. 4. Experimental UV/vis spectrum of **CN-HEL** in a $CHCl_3$ solution (C = 1.5 x 10^{-5} M) compared to the simulated one (cam/B3LYP/6-31++g(d,p) or PBEPBE/6-31++g(d,p) with a continuum solvent model for $CHCl_3$).

Table 3

Selected dominant excitations and occupied–unoccupied MO pair contributions of **CN-HEL**, and comparison with experiment.

λ^{exp} (nm)^a	λ^{calc} (nm)^b	E (eV)	Electronic transition	Oscillator Strength (f)	Assignment MO	%
365	363	3.41	$S_0 \rightarrow S_1$	0.0001	HOMO-1→LUMO	41
					HOMO→LUMO+1	41
340	345	3.59	$S_0 \rightarrow S_2$	0.0789	HOMO→LUMO	56
290	297	4.17	$S_0 \rightarrow S_6$	0.6509	HOMO-2→LUMO	46

270	275	4.50	$S_0 \rightarrow S_8$	0.7717	HOMO-1→LUMO+2	44

[a] Absorption measured in $CHCl_3$ solution (1.5×10^{-5} mol.L^{-1}) at room temperature.
[b] Absorption calculated using DFT/cam/B3LYP/6-31++g(d,p).

Based on the DFT/PBEPBE/6-31++g(d,p) optimized chemical structure, Frontier molecular orbitals (FMOs) are deduced and presented in Fig. 5. HOMOs and LUMOs are mainly distributed over the π-system of the benzene rings and onto the nitrile groups. This trend is attributable to the mild push-pull effect of the Donor and Acceptor units, leading to effective electronic communication between the Helicene and the cyano groups.

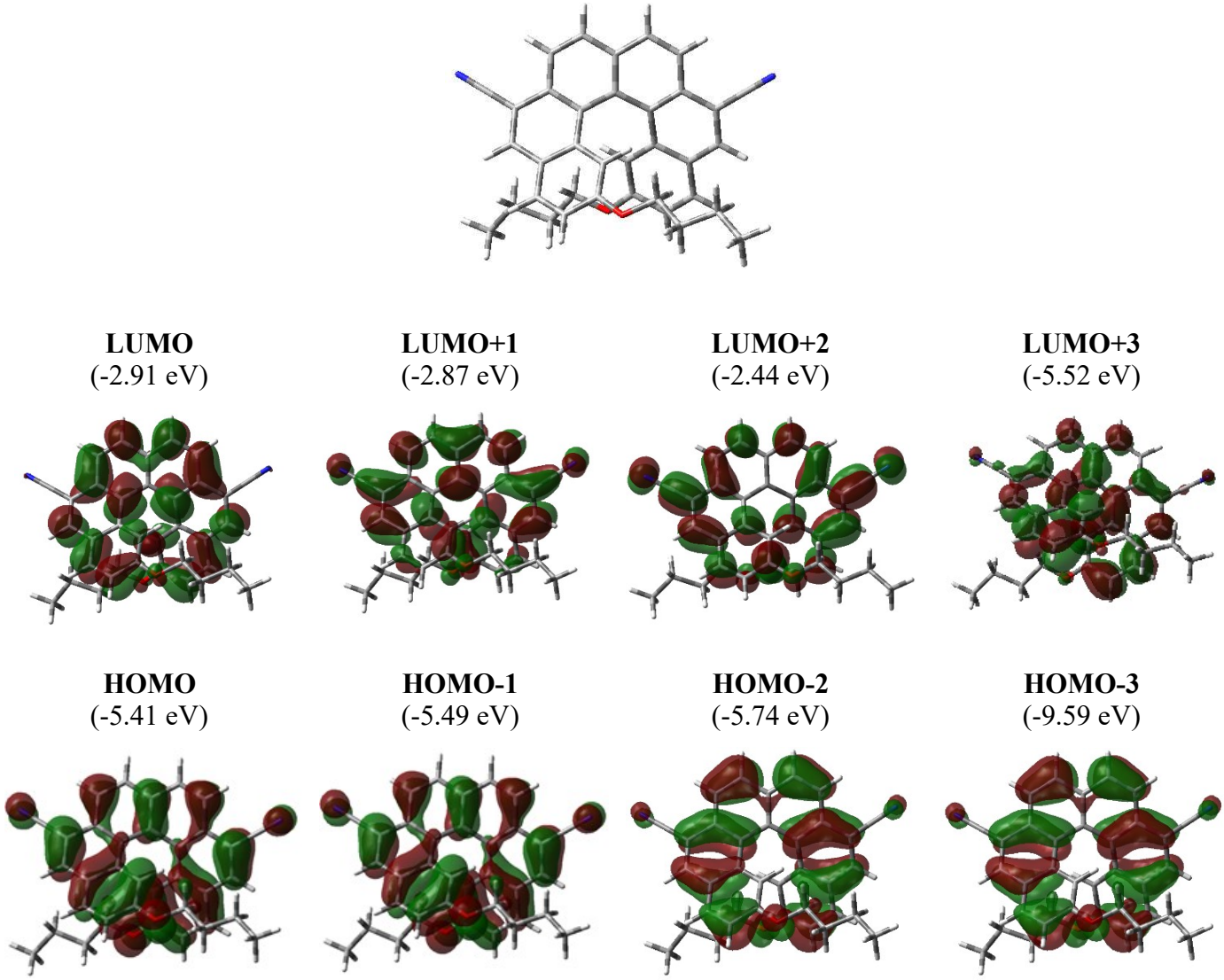

Fig. 5. Isosurfaces of MOs involved in selected transitions of **CN-HEL**. Values listed in the parentheses are the corresponding orbital energies, in eV.

The molecular electrostatic potential (MEP) surface is related to the electronic density, and it is a very useful method to understand the reactivity of a molecule. The MEP surface for **CN-HEL** (Fig. 6) was obtained from the optimized structure of **CN-HEL** by DFT/B3LYP/6-

31++g(d,p) and it comprises different colors, which increase in the order red<orange<yellow<green<blue. The negative (red and yellow) regions of the MEP are related to an abundance of electrons [24,25]. Whereas, the positive (blue) regions are related to an electron deficiency. Negative regions in **CN-HEL** were found around both nitrogen atoms belonging to C≡N groups. The positive regions are localized on the C-H and C-C groups of the phenyl rings. Also, a green color was observed around the butoxy groups, indicating a medium abundance of electrons.

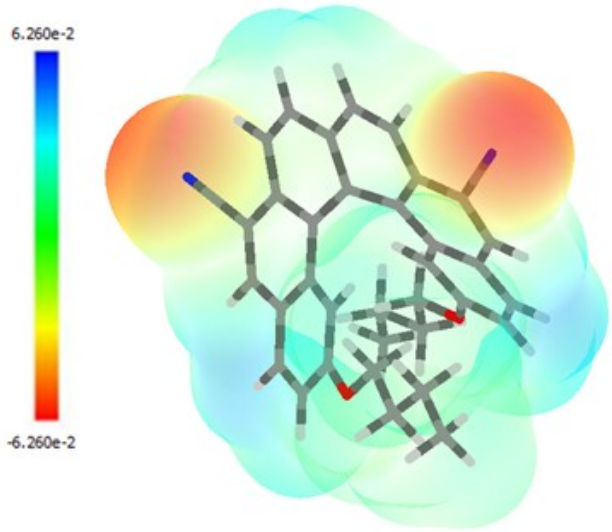

Fig. 6. Calculated electrostatic potential (MEP) surface of **CN-HEL**.

The experimental photoluminescence (PL) spectrum of **CN-HEL** was recorded from a dilute chloroform solution (C = 1 x 10^{-5} mol.L^{-1}) and in solid-state thin film prepared by spin coating (Fig. 7). Significant indigo fluorescence was observed upon excitation at λ_{exc} = 330 nm (see Table 4). **CN-HEL** displays structural emission bands at 398 nm and 422 nm, giving a stroke shift of 154 nm. In solid-state, there was a fluorescent band shift of approximately 25 nm, this effect is presumably associated with the symmetrical structure of **CN-HEL** which may promote strong π-π* stacking that hinder conformational changes such as causing an aggregation induced fluorescence enhancement. CIE chromaticity of the investigated **CN-HEL** in solution or in solid-state thin film shows that the material exhibits a blue emission in both states.

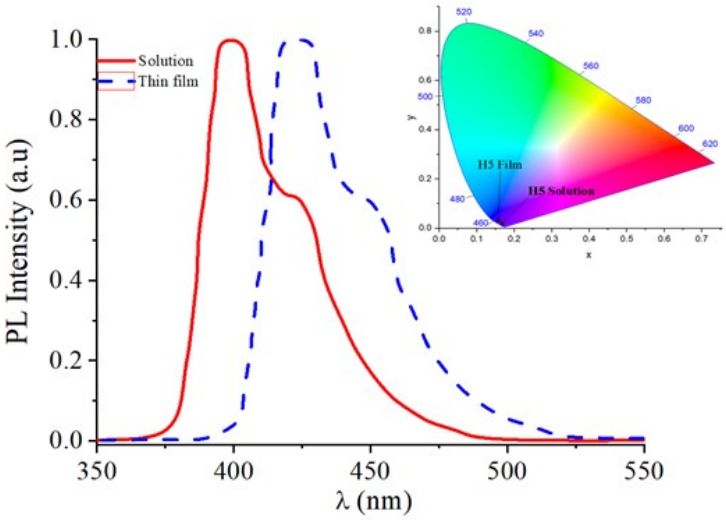

Fig. 7. Calculated and experimental in a dilute $CHCl_3$ solution (red line) and solid-state thin film (Blue dashed line) PL spectra of **CN-HEL**.

Table 4

Emission properties of **CN-HEL** in a dilute $CHCl_3$ solution and solid-state thin film.

Compound	Solution			Thin film	
	$\lambda_{ems}{}^{a}(\lambda_{exict})$ (nm)	FWHM[b] (nm)	Stokes shift (nm)	$\lambda_{ems}{}^{a}(\lambda_{exc})$ (nm)	FWHM[b] (nm)
CN-HEL	398 (330)	49	154	423 (330)	49

[a] Emission maxima measured in a $CHCl_3$ solution (1.6×10^{-5} mol.L^{-1}) at room temperature. Fluorescence excitation at 266 nm.
[b] Spectrum full width at half maximum.

To estimate the experimental HOMO and LUMO energy levels of **CN-HEL** by using cyclic voltammetry (CV), the material was dissolved in dichloromethane solution (5 mg/mL). Then, a three-electrode system was established in a quartz cell including an electrolyte solution, consisting of *n*-Bu_4NPF_6, with a concentration around 0.1 M under inert atmosphere. Oxidation and reduction potentials of the corresponding helicene were investigated at the 100 mV.s^{-1} as the scan rate. Cyclic voltammogram (Fig.8) shows that **CN-HEL** was oxidized at 1.53 V (*vs* saturated calomel electrode [SCE]) and reduced at -1.01 V, irreversibly. HOMO and LUMO energy levels were calculated by using the following formula [26,27].

$$E_{HOMO}\ (I_P, \text{ ionization potential}) = -\ (V_{onset\text{-}ox} - V_{FOC} + 4.8)$$

$$E_{LUMO}\ (E_A, \text{ electron affinity}) = -\ (V_{onset\text{-}red} - V_{FOC} + 4.8)$$

Where V_{FOC} means the ferrocene half-wave potential (0.494 V), measured versus a saturated calomel electrode (Ag/AgCl). HOMO and LUMO energy levels were measured as -5.83 eV and -3.29 eV, respectively (see Table 5). The electronic band gap ($E_{g\text{-}el}$) of the Helicene was found to be 2.54 eV as it has been calculated according to the empirical formula:

$$E_{g\text{-}el} = (E_{LUMO} - E_{HOMO})\ \text{eV}$$

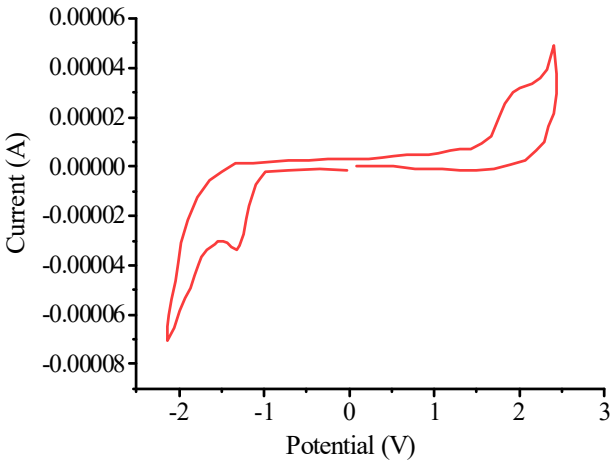

Fig. 7. CV spectrum of compound **CN-HEL** in 0.1 M (n-Bu)$_4$NPF$_6$/CH$_2$Cl$_2$ at a scanning rate of 100 mV/s.

Table 5
Electrochemical onset potentials and electronic energy levels of **CN-HEL**.

Helicene	$V_{onset\text{-}ox}$ (V)	$V_{onset\text{-}red}$ (V)	E_{HOMO} (eV)	E_{LUMO} (eV)	$E_{g\text{-}el}$ (eV)
CN-HEL	1.53	-1.01	-5.83	-3.29	2.54

In order to explore the non-covalent interactions (NCI) on the synthesized Helicene, reduced density gradient (RDG) analysis was undertaken on its optimized chemical structure with the Multiwfn software [28]. The iso-surface density and NCI diagram scatter obtained by plotting RDG *versus* the electron density (ρ) are deduced using the visual molecular dynamics (VMD) software (version 1.9.1) [29]. The obtained iso-surface density plots and NCI scatter diagrams were presented in Fig. 8. The false obtained colour can distinguish three types of interactions; blue colour indicates strong attractions (Hydrogen bond), red colour indicates the existence of strong repulsion interactions usually due to steric effects, and the green colour indicates the existence of intermediate interactions (Van der Waals). From Fig. 8b, we can note that ((λ_2) ρ < - 0.02) no scatter is shown for the low RDG values (RDG < 0.5 a.u), which indicate the absence of hydrogen bonding attraction. Meanwhile, a medium interaction type Van der Waals and strong repulsion due to steric effects are detected. The high degree of Van der Waals interactions and the existence of the steric effects induce the formation of a partial half elliptical slab on the center of the helical molecule as it is shown in the iso-surface density plots (Fig. 8a). In addition to that, a strong repulsion is observed in the center of the π-ring system.

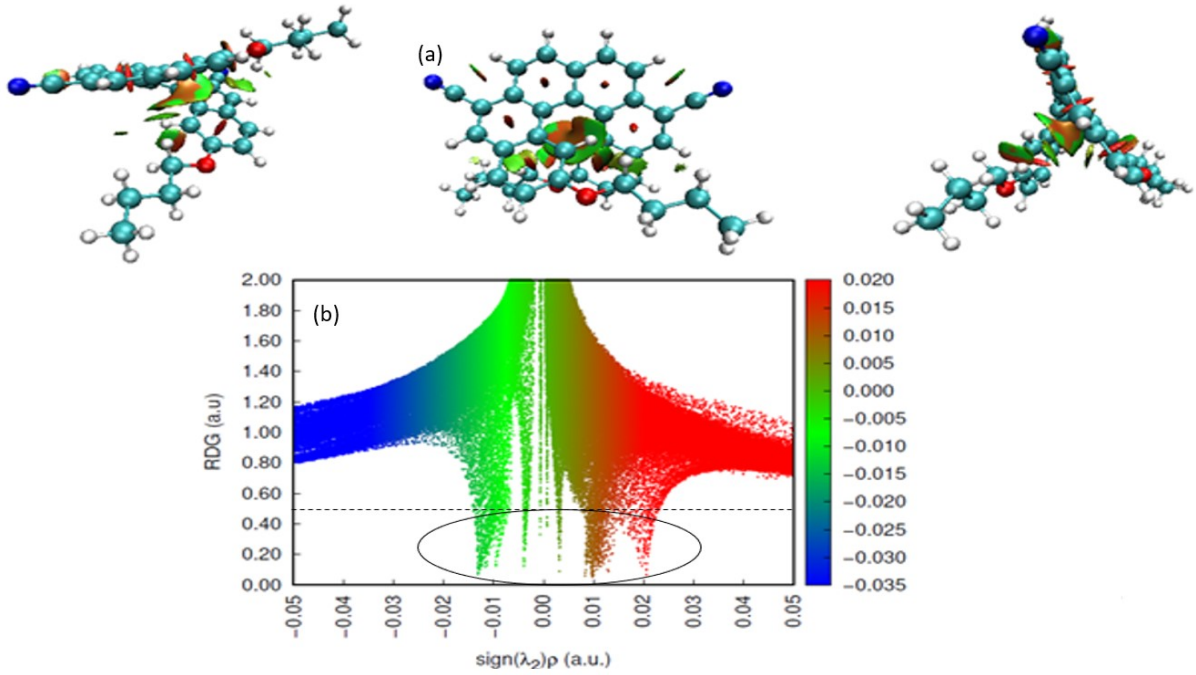

Fig. 1. (a) Reduced density gradient (RDG) analysis of the **CN-HEL** for different sides of view. (b) Non-covalent interaction (NCI) scatter diagram of **CN-HEL**.

4. Conclusion

A straightforward and high-yielding synthetic route to 2,15-dibutoxy-6,11-dicyano[6]Helicene has been described. The target Helicene was successfully characterized using different spectroscopic techniques including ^{1}H and ^{13}C NMR, FT-IR, UV-vis and photoluminescence. Its HOMO and LUMO energy levels have been evaluated showing an impressive electrochemical behavior. Photophysical properties of the Helicene have been experimentally examined and compared to calculated ones by DFT and TD-DFT simulations indicating a strong absorption in the UV region and a fluorescence emission in the visible area. Grafting butoxy and cyano groups in defined rings of the helical scaffold resulted in a significant intramolecular charge transfer (ICT) within the conjugated hexacyclic framework. Furthermore, based on the DFT calculations of the HOMO-LUMO energy levels, this compound can be potentially of interest as a hole-transporting unit.

5. Experimental section

5.1. General methods

All experiments were performed under an atmosphere of dry argon. Reagents purchased from commercial suppliers were tested for purity before use. Solvents were purchased from Aldrich and freshly distilled under argon from magnesium (Methanol) or from phosphorus pentoxide (tetrachloromethane). Irradiation reactions were conducted using a mercury vapor lamp (500 W, Hanovia). Column chromatography purifications were performed over silica gel obtained from Silicycle Chemical Division (40-63 nm; 230-240 mesh). ^{1}H and ^{13}C NMR spectra were recorded on a Bruker AM 300 and 400. Chemical shifts of ^{1}H and ^{13}C NMR were reported in parts per million (ppm) relative to Me_4Si as an external standard. UV-vis spectroscopy was conducted on a Varian Cary 5000 spectrometer. The electrochemical studies were carried out under argon using an Eco Chemie Autolab PGSTAT 30 potentiostat for voltammetric measurements, connected to a conventional three-electrode cell: the working electrode was a platinum microdisk, the reference electrode was a saturated calomel electrode and a platinum wire as the counter electrode. Melting point values were measured on a Sanyo Gallenkamp apparatus and are uncorrected.

*5.2. Experimental procedure for the preparation of (2Z,2'Z)-2,2'-(naphthalene-2,7-diyl)bis(3-(p-butoxyphenyl)acrylonitrile (**3**)*

In a nitrogen filled two necked 50-mL flask, were introduced 300 mg (1.4 mmol) of 2,7-bis(cyanomethyl)naphtalene (**2**), 0.5 mL (2.8 mmol) of 4-butoxybenzaldehyde and 15 mL of anhydrous methanol. The mixture was stirred at 0 °C for 20 min, and then 305 mg of sodium methoxide (5.6 mmol) was added in small portions. The resulting reaction mixture was stirred for 30 min at 0 °C, then for 6 h at room temperature. The precipitate that formed was filtered on a fritted glass, washed with water and dried to give the desired diarylethylene **3** as a yellow pure solid in 93% yield; mp = 135-137 °C; ^{1}H NMR (400 MHz, $CDCl_3$): δ (ppm) : 1.00 (t, J = 7.2 Hz, 6H, $2CH_3$), 1.51-1.57 (m, 4H), 1.79-1.85 (m, 4H), 4.04 (t, J = 6.4 Hz, 4H, $2CH_2$-O), 7.00 (d, J = 8.4 Hz, 4H), 7.63 (s, 2H), 7.77 (d, J = 8.8 Hz, 2H), 7.88 (d, J = 8.8 Hz, 2H), 7.94 (d, J = 8.8 Hz, 4H), 8.18 (s, 2H); ^{13}C NMR (100 MHz, $CDCl_3$): δ (ppm) : 13.83 ($2CH_3$), 19.22 ($2CH_2$), 31.19 ($2CH_2$), 67.97 ($2CH_2$-O), 108.02 (2C), 114.96 (4CH), 118.53 (2CN), 123.55 (2CH), 125,.85 (2CH), 126.22 (2CH), 128.54 (2CH), 131.39 (4CH), 132.80 (C), 133.21 (2C), 133.28 (C), 142.35 (2C), 161.28 (2C-O).

*5.3. Experimental procedure of the photocyclization of **3** into 2,15-dibutoxy-6,11-dicyano[6]Helicene (**CN-HEL**)*

150 mg of **3** (0.28 mmol) and 152 mg of iodine (0.59 mmol) were dissolved in 1.2 L of toluene. The mixture was degassed and purged with argon for 30 min, and then propylene oxide (50 eq.) was added. The solution was irradiated using a high-pressure Hg-vapor lamp (500 W) for 7 h, with maintaining the flow of argon throughout the irradiation. After completion, the solvent was removed under reduced pressure and the crude product was chromatographed over a flash silica gel column (cyclohexane : EtOAc 98:02, *v*/*v*) leading to 126 mg of pure **CN-HEL** in 85% yield as a yellow solid; mp = 137-139 °C; ^{1}H NMR (400 MHz, $CDCl_3$): δ (ppm) : 0.89 (t, J = 7.6 Hz, 6H, 2CH_3), 1.24-1.31 (m, 4H, 2CH_2), 1.45-1.49 (m, 4H, 2CH_2), 2.71-2.77 (m, 2H), 3.11 (m, 2H), 6.91 (s, 2H, $H_{1/16}$), 7,00 (d, J = 8.8 Hz, 2H, $H_{3/14}$), 7.79 (d, J = 8.8 Hz, 2H), 8.20 (d, J = 8.4 Hz, 2H), 8.36 (s, 2H, $H_{5/12}$), 8.47 (d, J = 8.4 Hz, 2H, $H_{7/10}$); ^{13}C NMR (100 MHz, $CDCl_3$): δ (ppm) : 13.69 (2CH_3), 19.03 (2CH_2), 30.69 (2CH_2), 67.14 (2CH_2-O), 106.16 (2C), 108.13 (2CH), 118.46 (2CN), 119.70 (2CH), 123.74 (C), 124.67 (2C), 125.03 (2CH), 127.10 (2C), 128.80 (2CH), 129.63 (2C), 129.73 (2CH), 133.16 (2C), 133.78 (C), 135.11 (2CH), 159.71 (2C-O).

References

[1] M.S. Newman, D. Lednicer, The synthesis and resolution of hexahelicene, J. Am. Chem. Soc. 78 (1956) 4765–4770. doi.org/10.1021/ja01599a060

[2] M.A. Shcherbina, X.B. Zeng, T. Tadjiev, G. Ungar, S.H. Eichhorn, K.E.S. Phillips, T.Z. Katz, Hallow six-stranded helical columns of a Helicene, Angew. Chem., Int. Ed. 48 (2009) 7837–7840. doi.org/10.1002/anie.200903658

[3] J. Kelber, M.F. Achard, F. Durola, H. Bock, Distorted arene core allows room–temperature columnar liquid–crystal glass with minimal side chains, Angew. Chem. Int. Ed. 51 (2012) 5200–5203. doi.org/10.1002/anie.201108886

[4] Y.Y. Xu, G. Yang, H.Y. Xia, G. Zou, Q.J. Zhang, J.G. Gao, Enantioselective synthesis of helical polydiacetylene by application of linearly polarized light and magnetic field, Nat. Commun. 5 (2014) 5050. doi.org/10.1038/ncomms6050

[5] D.J. Weix, S.D. Dreher, T.J. Katz, [5]HELOL phosphite: a helically grooved sensor of remote chirality, J. Am. Chem. Soc. 122 (2000) 10027–10032. doi.org/10.1021/ja001904n

[6] S. Sakunkaewkasem, A. Petdum, W. Panchan, J. Sirirak, A. Charoenpanich, T. Sooksimuang, N. Wanichacheva, Dual-analyte fluorescent sensor based on [5]Helicene derivative with super large stokes shift for the selective determinations of Cu^{2+} or Zn^{2+} in buffer solutions and its application in a living cell, ACS Sensors 5 (2018) 1016-1023. doi.org/10.1021/acssensors.8b00158

[7] A. Desmarchelier, X. Caumes, M. Raynal, A. Vidal-Ferran, L. Van, W.N.M. Piet, L. Bouteiller, Correlation between the selectivity and the structure of an asymmetric catalyst built on a chirally amplified supramolecular helical scaffold, J. Am. Chem. Soc. 138 (2016) 4908–4916. doi.org/10.1021/jacs.6b01306

[8] J.J. Li, M. Du, Z.Q. Zhao, H.W. Liu, Cyclopolymerization of disiloxane-tethered divinyl monomers to synthesize chirality-responsive helical polymers, Macromolecules 49 (2016) 445–454. doi.org/10.1021/acs.macromol.5b02142

[9] J.E. Field, G. Muller, J.P. Riehl and D. Venkataraman, Circularly polarized luminescence from bridged triarylamine helicenes, J. Am. Chem. Soc. 125 (2003) 11808–11809. doi.org/10.1021/ja035626e

[10] M. Li, L.H. Feng, H.Y. Lu, S. Wang, C.F. Chen, Tetrahydro[5]helicene-based nanoparticles for structure-dependent cell fluorescent imaging, Adv. Funct. Mater. 24 (2014) 4405– 4412. doi.org/10.1002/adfm.201400199

[11] Y. Yang, B. Rice, X. Shi, J.R. Brandt, R.C. da Costa, G.J. Hedley, D. Smilgies, J.M. Frost, I.D.W. Samuel, A. Otero-de-la-Roza, E.R. Johnson, K.E. Jelfs, J. Nelson, A.J. Campbell, M.J. Fuchter, Emergent properties of an organic semiconductor driven by its molecular chirality, ACS Nano 11 (2017) 8329−8338. doi.org/10.1021/acsnano.7b03540

[12] Y. Nakakuki, T. Hirose, K. Matsuda, Logical design of small HOMO–LUMO gap: Tetrabenzo[*f,jk,mn,r*][7]helicene as a small-molecule near-infrared emitter, Organic Lett. 24, 2, (2022) 648-652. doi.org/10.1021/acs.orglett.1c04095

[13] S. Sahasithiwat, T. Sooksimuang, L. Kangkaew, W. Panchan, 3,12-Dimethoxy-5,6,9,10-tetrahydro-7,8-dicyano[5]helicene as a new emitter for blue and white organic light-emitting diodes, Dyes and Pigments 136 (2017) 754–760. doi.org/10.1016/j.dyepig.2016.09.042

[14] B.K. Mandal, T. Sooksimuang, C.H. Lee, R. Wang, Self-assembled, nano-structured octaalkoxy helicenocyanines, J. Porphyr. Phthalocya. 10 (2006) 140–146. doi.org/10.1142/S108842460600017X

[15] H. Kubo, T. Hirose, T. Nakashima, T. Kawai, J. Hasegawa, K. Matsuda, Tuning transition electric and magnetic dipole moments: [7]Helicenes showing intense circularly polarized luminescence, J. Phys. Chem. Lett. 12 (2021) 686−695. doi.org/10.1021/acs.jpclett.0c03174

[16] J.R. Brandt, X. Wang, Y. Yang, A.J. Campbell, M.J. Fuchter, Circularly polarized phosphorescent electroluminescence with a high dissymmetry factor from PHOLEDs based on a platinahelicene, J. Am. Chem. Soc. 138 (2016) 9743–9746. doi.org/10.1021/jacs.6b02463

[17] J.R. Brandt, F. Salerno and M.J. Fuchter, The added value of small-molecule chirality in technological applications, Nat. Rev. Chem. 1 (2017) 0045. doi.org/10.1038/s41570-017-0045

[18] A. Terfort, H. Görls, H. Brunner, The first helical-chiral phosphane ligands: ras-[5]- and ras-[6]-Heliphos, Synthesis (Mass) (1977) 79–86 . doi.org/10.1055/s-1997-1498

[19] S. Raouafi, B.H. Asghar, F. Aloui, Novel bis-nitrile grafted [6]Helicenes through a photochemical pathway: Chiroptical and photophysical properties, Journal of Molecular Structure 1225 (2021) 129087. doi.org/10.1016/j.molstruc.2020.129087

[20] J. Coates, Interpretation of infrared spectra, a practical approach, Encyclopedia of analytical chemistry, John Wiley & Sons, Ltd, 2006, pp. 1–23. doi.org/10.1002/9780470027318.a5606

[21] C.-Z. Wang, R. Kihara, X. Feng, P. Thueŕy, C. Redshaw, T. Yamato, Synthesis, structure and photophysical properties of pyrene–based [5]Helicenes: an experimental and theoretical study, Chemistry Select 2 (2017) 1436–1441. doi.org/10.1002/slct.201601327

[22] X. Jia, J. Nitsch, L. Ji, Z. Wu, A. Friedrich, F. Kerner, M. Moos, C. Lambert, T. B. Marder, Triarylborane-based helical donor–acceptor compounds: synthesis, photophysical, and electronic properties, Chem. Eur. J. 25 (2019) 1–14. doi.org/10.1002/chem.201902258

[23] H. Isla, N. Saleh, J.-K. Ou-Yang, K. Dhbaibi, M. Jean, M. Dziurka, L. Favereau, N. Vanthuyne, L. Toupet, B. Jamoussi, M.S.-Hooper, J. Crassous, Bis-4-aza[6]Helicene: A Bis-helicenic-2,2′-bipyridine with chemically triggered chiroptical switching activity, J. Org. Chem. 84 (2019) 5383−5393. doi.org/10.1021/acs.joc.9b00389

[24] K. Hamrouni, N. Hafedh, M. Chmeck, F. Aloui, Photooxidation pathway providing 15-bromo-7-cyano[6]helicene. Chiroptical and photophysical properties and theoretical investigation, J. Mol. Struct. 1217 (2020) 128399. doi.org/10.1016/j.molstruc.2020.128399

[25] A. Artigas, D. Hagebaum-Reignier, Y. Carissan, Y. Coquerel, Visualizing electron delocalization in contorted polycyclic aromatic hydrocarbons, Chem. Sci. 12 (2021) 13092-13100. doi.org/10.1039/D1SC03368A

[26] J. Pommerehne, H. Vestweber,W. Guss, R. F.Mahrt, H. Bassler, M. Porsch, J. Daub, Efficient two layer leds on a polymer blend basis, Adv. Mater. 7 (1995) 551–554. doi.org/10.1002/adma.19950070608

[27] J.L. Bredas, R. Silbey, D.S. Boudreaux, R.R. Chance, Chain-length dependence of electronic and electrochemical properties of conjugated systems: polyacetylene, polyphenylene, polythiophene, and polypyrrole, J. Am. Chem. Soc. 105 (1983) 6555-6559.

[28] T. Lu, F. Chen, Multiwfn: a multifunctional wavefunction analyzer, J. Comput. Chem. 33 (2012) 580–592. doi.org/10.1002/jcc.22885

[29] W. Humphrey, A. Dalke, K. Schulten, VMD: visual molecular dynamics, J. Mol. Graph. 14 (1996) 33–38. doi.org/10.1016/0263-7855(96)00018-5